Reprinted from The Journal of Physical Chemistry, 1993, 97.

Interaction of Low-Energy Electrons with SO_2 Layers on Ag(111): Comparison to Photochemistry

Laura A. Pressley, J. Kiss,† and J. M. White*

Department of Chemistry and Biochemistry, The University of Texas at Austin, Austin, Texas 78712

Miguel E. Castro

Department of Chemistry, Oklahoma State University, Stillwater, Oklahoma 74078

Received: June 25, 1992; In Final Form: November 9, 1992

The interaction of low-energy electrons (8–54 eV) with SO_2 layers on Ag(111) has been studied using temperature programmed desorption (TPD) and Auger electron spectroscopy (AES). For coverages up to one monolayer, the only electron-stimulated desorption (ESD) process is parent desorption, which has a cross section of 3.6 ± 0.8 × 10^{-17} cm^2 using 54 ± 1 eV electrons. This ESD process has an electron energy threshold of 18.0 ± 1.0 eV corresponding to ionization of the $6a_1$ molecular orbital of adsorbed SO_2. For coverages greater than one monolayer, ESD is accompanied by electron-induced decomposition (EID) and the total cross section for loss of SO_2 is ≈10^{-16} cm^2, independent of coverage up to 8 monolayers (ML). The differences between chemisorbed and physisorbed layers is attributed mainly to metal-induced quenching of electronically excited adsorbates, which is less important for those SO_2 molecules further from the metal. Compared to photon-driven desorption, electron-driven desorption follows a different excitation pathway, which we attribute to the formation of transient positive ions.

1. Introduction

Recently, the photon[1-3] and electron-induced[4-14] chemistry of molecules adsorbed on metal and semiconductor surfaces has been pursued by the scientific community. The motivation is both fundamental and practical; bond-specific chemistry issues, mechanistic issues, and energy-transfer issues are of fundamental interest, while practical considerations relate to the use of optical and particle processing of electronic materials and device structures and the use as a tool for the preparation of interesting intermediates relevant to catalysis.[7,10-13,15-18]

Recently we reported that the *thermal* properties of SO_2 adsorbed on Ag(111) are completely reversible, with desorption peaks at 180, 145, and 130 K attributed to chemisorbed, compressed, and physisorbed layers, respectively.[19a,b] Irradiation of the chemisorbed layer with ultraviolet (UV) photons from a Hg arc lamp (4.9–3.5 eV) leads exclusively to molecular SO_2 desorption. The photodesorption cross section follows the optical absorbance of the substrate and has a local maximum of 2.8 ± 0.2 × 10^{-20} cm^2 at the silver bulk plasmon excitation near 3.8 eV. The photodesorption rate increases monotonically with SO_2 coverage up to 1 ML, but above 1 ML, it decreases sharply.

A long term goal of our laboratory is elucidation of nonthermal excitation pathways by which surface chemistry can be manipulated, particularly the surface chemistry of adsorbates of technological and/or environmental relevance. The environmental significance of SO_2 is well known; e.g., it is a product of the smelting of metal ores and the combustion of coal. In the atmosphere, it reacts with water to form acid rain.[20a] The gas-phase photophysical and photochemical properties of SO_2 are complex and widely studied,[20b-24] providing a rich background for surface investigations.

In this paper, we report that low-energy electrons (8–54 eV) induce interesting surface chemistry in adsorbed SO_2, and we compare these results with earlier work using photons to drive the surface processes.[19] Briefly, and as for photon-driven chemistry, electron irradiation of coverages up to one monolayer results *exclusively* in electron stimulated desorption (ESD) of SO_2 with an electron energy threshold of 18.0 ± 0.7 eV and a cross section of 3.6 ± 0.8 × 10^{-17} cm^2 at 54 eV. However, unlike photon-driven chemistry of SO_2,[19] there is no evidence for electron stimulated desorption from defect sites. For multilayers, both parent ESD and electron induced decomposition (EID) are readily observed. The appearance of EID in multilayers is ascribed to slower quenching of molecules excited further from the Ag substrate. We discuss the differences brought about by two different excitation pathways, transient positive ion formation upon electron impact and transient negative ion formation upon photon-driven hot substrate electron attachment to the adsorbate.

2. Experimental Section

All experiments were carried out in an ultrahigh vacuum chamber described in detail elsewhere.[25] Briefly, the chamber has a quadrupole mass spectrometer for temperature programmed desorption (TPD) and residual gas analysis (RGA) and a double pass cylindrical mirror analyzer (CMA) for Auger electron spectroscopy (AES). The chamber is ion pumped and has auxiliary titanium sublimation and 170 L/s turbomolecular pumps. The working base pressure during the experiments reported here was 1.5 × 10^{-10} Torr.

The procedure for mounting the Ag(111) crystal has been described previously.[26] The sample could be cooled to 100 K with liquid nitrogen and resistively heated to 1000 K. The sample temperature was measured using a chromel–alumel thermocouple spot welded to a tantalum loop that was inserted into a hole drilled in the side of the crystal. The Ag(111) crystal was cleaned by cycles of (Ar^+) sputtering and annealing (≈700 K) until no impurities were observed by AES.

SO_2, 99% pure, was further purified by freeze–pump cycles at 77 K, and the purity was verified by RGA. SO_2 was admitted into the chamber using a stainless steel capillary array doser. For exposures, the chamber partial SO_2 pressure was increased to 2 × 10^{-10} Torr with the front face of the sample turned away from the doser. To initiate the dose, the sample was then quickly rotated to face the doser. The distance between the sample and the doser was ~0.50 cm.

† Permanent address: Reaction Kinetics Research Group of the Hungarian Academy of Sciences, University of Szeged, P.O. Box 105, Szeged, Hungary.

0022-3654/58/2097-0902$04.00/0

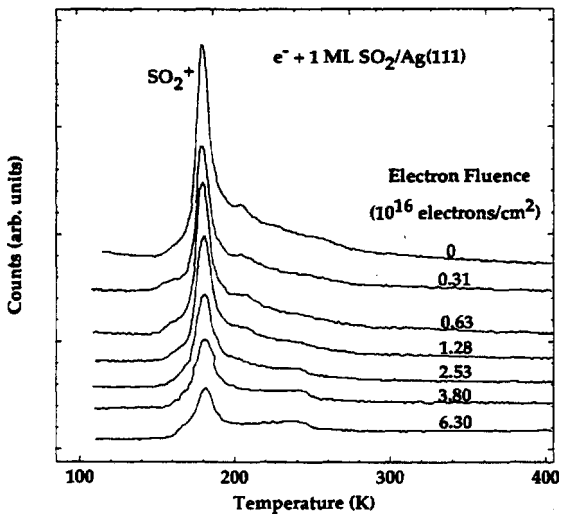

Figure 1. Postirradiation TPD of SO_2 from Ag(111) for several electron fluences as indicated on each curve. The incident electron energy was 54 ± 1 eV. The temperature ramp rate was 2.1 K/s.

The mass spectrometer filament was used as the electron source. During the fluence and electron energy dependence experiments, the current to the Ag(111) sample was maintained at ~2 μA; the irradiation times were varied to change the fluence. When not used for TPD, ESD, or EID measurements, the filament was maintained at a low emission current (0.38 mA) to minimize unwanted beam-induced effects. The electron energy distribution, measured using the CMA, peaked at 54 eV with a full width at half-maximum (fwhm) of 1 eV.[25] Throughout this paper, we use the fwhm as an estimate of the uncertainty in the electron energy. For the ESD and EID experiments, the sample was placed in line-of-sight with the mass spectrometer. During electron irradiation, desorption of products was monitored with the quadrupole operating in a multiplex mode. Electron fluxes were estimated by measuring the electron current to the crystal with respect to ground. This does not take into account either primary electrons reflected from the sample or secondary electrons generated within the substrate and ejected into vacuum. Thus, as discussed elsewhere,[11] the cross sections reported here represent upper limits. For the TPD measurements, the sample was turned about 30° away from the line-of-sight position to minimize contributions of ESD and EID artifacts.

3. Result

We first focus on the electron-induced chemistry of 1 ML of SO_2, prepared by flashing 2 ML to 145 K. This procedure desorbs the physisorbed and compressed layers[19a] and anneals the remaining SO_2, an important consideration in this system.[19b] Compressed and multilayer coverages are discussed in section 3.2.

3.1. Electron Irradiation of Monolayer SO_2. Starting with monolayer SO_2, Figure 1 shows the TPD after exposure to various electron fluences (electrons/cm^2). The incident electron energy is 54 ± 1 eV. In the absence of electron irradiation (top spectrum), there is, consistent with earlier work,[19] a peak at 180 K due to desorption of the chemisorbed layer. There is also a commonly observed (ref 19 and references cited therein) high-temperature tail above 200 K attributed, in part, to desorption from defects. It accounts for about 15% of the total TPD peak area and may include a small contribution from the backside of the sample. However, since desorption always occurs in this region, even for the smallest doses,[19] most is coming from the front surface. All the SO_2 adsorption and desorption occurs with no intraadsorbate bond breaking.

The SO_2 TPD peak area decreases with increasing electron fluence, with no change in the peak temperature. There is no evidence for bond breaking within SO_2. During irradiation, the only product ejected is SO_2, i.e., SO_2^+, and its cracking fragments are detected with the QMS (see Figure 3a and Discussion). After irradiation, only parent desorption is observed in TPD, and AES analysis following TPD shows no detectable levels of sulfur or oxygen remaining on the surface. We conclude that there is no intraadsorbate bond cleavage and that electron irradiation of monolayer SO_2 results *exclusively* in desorption of parent molecules.

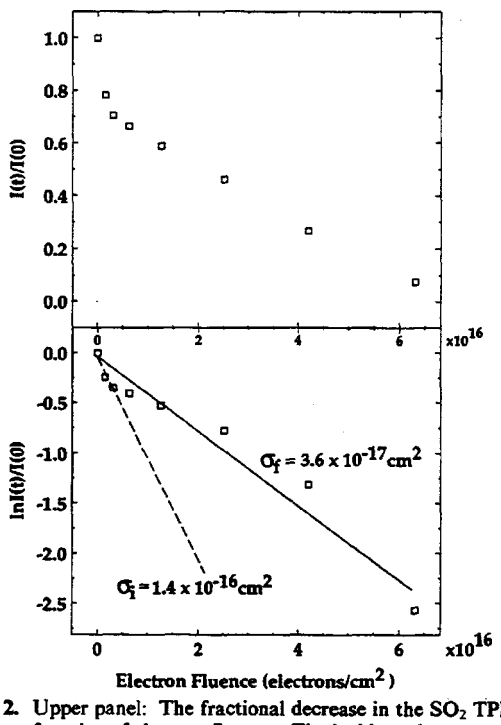

Figure 2. Upper panel: The fractional decrease in the SO_2 TPD peak areas as a function of electron fluence. The incident electron energy is 54 ± 1 eV, and the initial SO_2 coverage is 1 ML. Lower panel: Semilogarithmic plot of the data from the upper panel. High and low cross-section regions are indicated.

It is important that, after irradiation, only minor changes appear in the high-temperature tail of the TPD, indicating little ESD of SO_2 from defect sites. This was verified by the following experiment (not shown). A surface covered with 2 ML of SO_2 was flashed to 190 K, leaving only SO_2 which desorbs in the high-temperature tail. During electron irradiation, 6.3×10^{16} electrons/cm^2, there was no increase in the gas-phase SO_2 background signal and, after irradiation, TPD showed, within experimental error, no loss of SO_2. We conclude that ESD from defect sites is small compared to desorption from flat Ag(111) sites. This is in marked contrast with photon stimulation, where the reported photodesorption cross section for SO_2 adsorbed on defect sites is about 4 times that for desorption from terrace sites.[19]

Based on TPD peak areas, the upper panel of Figure 2 shows the fraction of SO_2 left on the surface, $I(t)/I(0)$, as a function of electron fluence, F_e. The contribution from defect sites has been subtracted. Assuming first-order kinetics, the ESD cross section is calculable from[27]

$$-(dN/dt) = n\sigma(E)N \qquad (1)$$

where N is the total coverage of adsorbed species (molecules/cm^2), $\sigma(E)$ is the electron energy dependent cross section for electron induced processes (cm^2), and n is the flux of electrons (electrons/cm^2-s). Equation 1 can be integrated to yield

$$\ln\{N(t)/N(0)\} = -n\sigma(E)t = -(i_e t/eA)\sigma(E) = -F_e\sigma(E) \qquad (2)$$

where $N(t)/N(0)$ is the ratio of the SO_2 TPD peak areas (subtracting defect desorption) after and before irradiation, t is

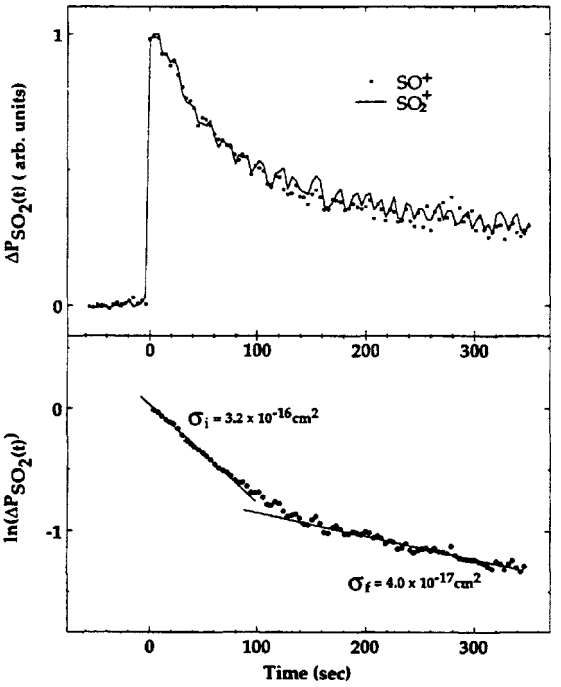

Figure 3. Upper panel: SO_2^+ (solid line) and SO^+ (dots) signals measured with QMS during electron irradiation (54 ± 1 eV) of one monolayer of SO_2 on Ag(111) at 105 K. Lower panel: Semilogarithmic plot of data from the upper panel. Solid curves are fits to two exponential decays.

time (s), i_e is the current density (A/cm^2), e is the electron charge, and F_e is the electron fluence (nt).

As shown in the lower panel of Figure 2, and more clearly in other data below, the loss of SO_2 is not linear with respect to electron fluence; there is always a faster decay early in the process (low fluence). Thus, the process cannot be represented by a single simple first-order kinetic model; as for photon driven desorption,[19b] the sum of at least two first-order processes is required. The two lines in the lower panel of Figure 2 show our estimates for the early, $\sigma_i = 1.4 \pm 0.8 \times 10^{-16}$ cm^2, and late, $\sigma_f = 3.6 \pm 0.8 \times 10^{-17}$ cm^2, cross sections (upper limits). Later (Discussion section) we propose a model involving electron-induced reorientation of SO_2 to account for this change.

Figure 3a shows the isothermal (105 K) gas-phase time-dependent SO_2^+ (line) and SO^+ (dots) signals, measured during electron irradiation. For $t < 0$ seconds, the sample is off the line-of-sight position with the mass spectrometer and is, thus, minimally dosed with electrons. At $t = 0$ seconds, electron dose is initiated by rotating the sample into the line-of-sight position. There is a sharp rise in both signals, and when normalized at the maximum, they track each other faithfully. Furthermore, if the SO^+ desorption trace is corrected for SO_2 fragmentation, no residual signal remains. Therefore, gas-phase products measured during irradiation confirm our conclusion, based on TPD and AES, that electron irradiation of a monolayer results in desorption, but no dissociation, of chemisorbed SO_2.

The data in the upper panel of Figure 3 are plotted in semilogarithmic (first order) form in the lower panel of Figure 3. Following Madey and Yates,[27] the ESD cross section can be calculated from the following equation:

$$I = i_e \sigma N \tag{3}$$

where I is the intensity of the desorbing species, in our case, SO_2^+. Substituting eq 3 into eq 1 gives

$$dI/dt = -n\sigma I \tag{4}$$

and yields

$$\ln \{I(t)/I_{max}\} = -n\sigma t \tag{5}$$

The slope of $(I(t)/I_{max})$ versus time gives the cross section.

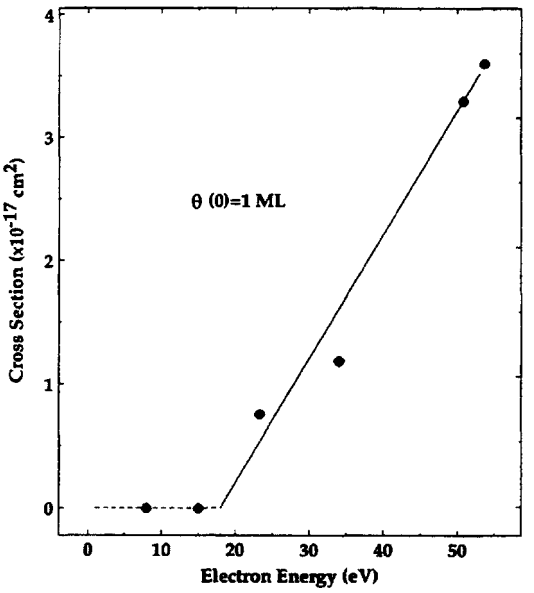

Figure 4. The ESD cross section as a function of electron energy. Electron fluence was constant at 2.0×10^{16} electrons/cm^2, and the lines through the data indicate an effective threshold at about 18 eV.

Confirming the TPD data, the plot of eq 5 is nonlinear (lower panel of Figure 3) but can be fit as the sum of two independent first-order processes. The initial slope indicates a relatively fast initial exponential decay, $\sigma_i = 3.2 \times 10^{-16}$ cm^2, whereas the slower channel, evident at longer irradiation times, gives $\sigma_f = 4.0 \times 10^{-17}$ cm^2. These two estimates, based on a much higher number of data points, are more reliable but certainly consistent with the data of Figure 2.

Figure 4 shows how the cross section varies with electron energy. With a constant initial coverage (1 ML) and fluence (2.5×10^{16} electrons/cm^2), i.e., sufficient to get into the slower desorption region, cross section values were obtained from postirradiation TPD areas (as in Figure 2). The electron energy was changed by varying a negative bias voltage between the sample and ground. Within our experimental uncertainty, there is no measurable ESD cross section at or below 15 eV. Above about 20 eV, the cross section increases monotonically with electron energy. By linear extrapolation, we estimate a threshold for molecular desorption of 18.0 ± 1 eV. In passing, it is noteworthy that the observation of an experimental threshold, under conditions where the measured sample current is high enough to detect cross sections of order 10^{-20} cm^2, is good evidence that artifacts are not significant. The data in Figure 4 are consistent with ionization from the $6a_1$ molecular orbital of SO_2 by a first-order, direct ionization process. This will be considered further in the Discussion section.

3.2. Electron Irradiation of Coverages Greater Than 1 ML. *3.2.1. Fragments Retained on the Surface.* For coverages above one monolayer, electron-induced decomposition of SO_2 occurs. Between 1 and 4 ML, Figure 5 summarizes SO_2 TPD before (solid lines) and after (dotted curves) irradiation with 1.26×10^{16} electrons/cm^2 at 54 ± 1 eV. Compared to a monolayer, irradiation of multilayers leads to TPD spectra in which a greater fraction of the 180 K chemisorbed peak is lost. Thus, the presence of the multilayer somehow promotes the loss of the *chemisorbed* SO_2. As a function of initial SO_2 coverage, Figure 6 summarizes the amount of chemisorbed ($T_p = 180$ K) SO_2 left on the surface, after irradiation with 1.26×10^{16} electrons/cm^2. Clearly, between 1 and 2 ML, the amount of chemisorbed SO_2 retained on the surface sharply decreases. Between 2 and 8 ML, the chemisorbed remainder is approximately constant, 0.26 ML, but it may be rising slowly.

Interestingly (Figure 5), desorption assigned to the compressed layer structure ($T_p = 145$ K), see ref 19, is absent in the TPD spectra taken after electron exposure. By way of comparison,

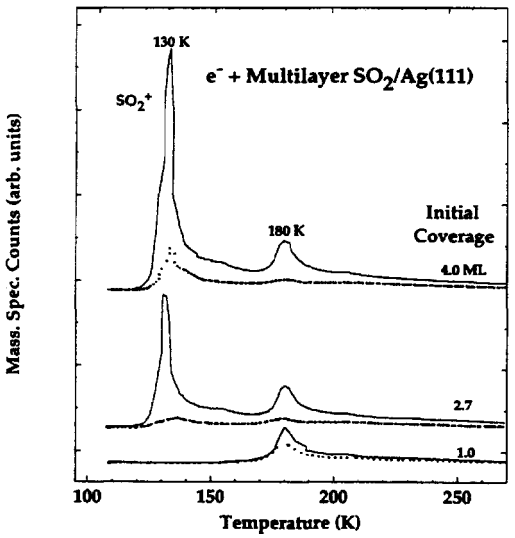

Figure 5. SO_2 TPD spectra as a function of initial coverage before (solid lines) and after irradiation (dots) with 1.2×10^{16} electrons/cm^2. The incident electron energy was 54 ± 1 eV.

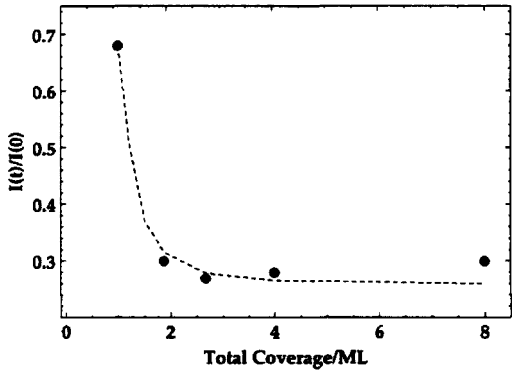

Figure 6. As a function of initial coverage, the fraction of SO_2 left in the *chemisorbed* SO_2 TPD peak after irradiation with a fluence of 1.2×10^{16} electrons/cm^2.

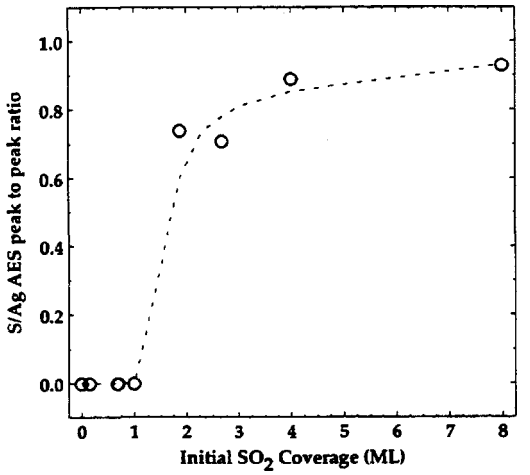

Figure 7. S(152 eV)/Ag(302 eV) AES peak-to-peak ratio, after electron dosing and annealing to 500 K, as a function of initial SO_2 coverage.

the compressed and chemisorbed SO_2 TPD areas are both suppressed on a sulfur-covered Ag(111) surface (not shown). That atomic sulfur plays a role in Figure 5 is confirmed as follows.

Unlike coverages up to one monolayer, AES measurements, after TPD to 500 K of electron-irradiated multilayers to remove remaining parent, show a substantial amount of atomic sulfur. As shown in Figure 7, the S/Ag AES signal ratio increases sharply between 1 and 2 ML and then levels off. Using standard AES atomic sensitivity factors, we calculate a S/Ag atomic ratio of

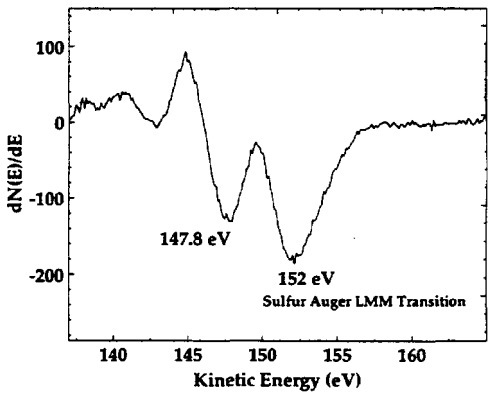

Figure 8. Derivative AES spectrum of the S(LMM) region.

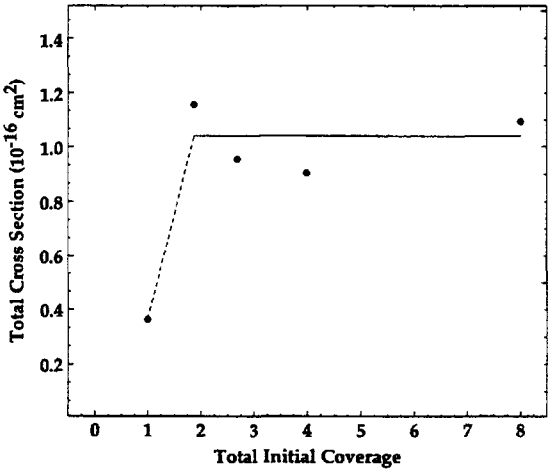

Figure 9. Total cross section (based on postirradiation TPD areas) for the interaction of low-energy electrons with SO_2 on Ag(111) as a function of initial coverage. Below one monolayer, the cross section is exclusively the result of neutral molecular desorption whereas above one monolayer it includes desorption and dissociation of ions and neutrals.

0.30 ± 0.05 at 8 ML (Figure 7). There is also a little oxygen, which is difficult to quantify due to interference with the Ag Auger transitions at about 506 eV. From this AES data, we conclude that electron-induced decomposition occurs when, and only when, multilayers are adsorbed. We speculate that this decomposition is accompanied by a shift of the remaining SO_2 from a chemisorbed to a physisorbed configuration. In this way, the effective cross section for loss of chemisorbed SO_2 rises when multilayers are present.

Parenthetically, the derivative Auger spectrum between 137 and 165 eV for the remaining sulfur is, itself, quite interesting (Figure 8). Referenced to the silver AES transition at 351 eV, two peaks are readily identified (147.8 and 152 eV). To discuss these, we first note that Salmeron et al.[28] have correlated the line shapes of sulfur, carbon, and oxygen Auger transitions on a number of metallic substrates to the degree of ionicity in the adsorbate–metal bond. The possibility of bulk plasmon excitation must also be considered since the energy required to excite the silver bulk plasmon is 3.97 eV[29] and the two AES peaks are separated by 4.2 eV. Excitation of electrons in the Ag 4d band (3.9 eV), i.e., a shake-up satellite, is also possible.

Returning to the dissociation of SO_2, we have established a major distinction in the electron-induced chemistry of chemisorbed and physisorbed layers. We now discuss the electron-induced dissociation and desorption of SO_2 in multilayers (T_p = 130 K). Based on SO_2 TPD areas, Figure 9 shows the total cross section for the electron-induced removal of SO_2 as a function of the initial coverage (1–8 ML). The fluence and electron energy were fixed at 1.26×10^{16} electrons/cm^2 and 54 ± 1 eV, respectively. For initial coverages of 1 ML, the only electron-induced process

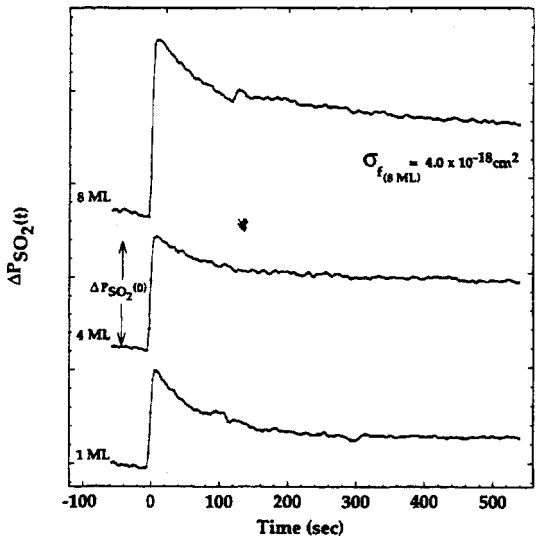

Figure 10. ESD trace of SO_2^+ for the indicated initial coverages. The incident electron energy is 54 ± 1 eV.

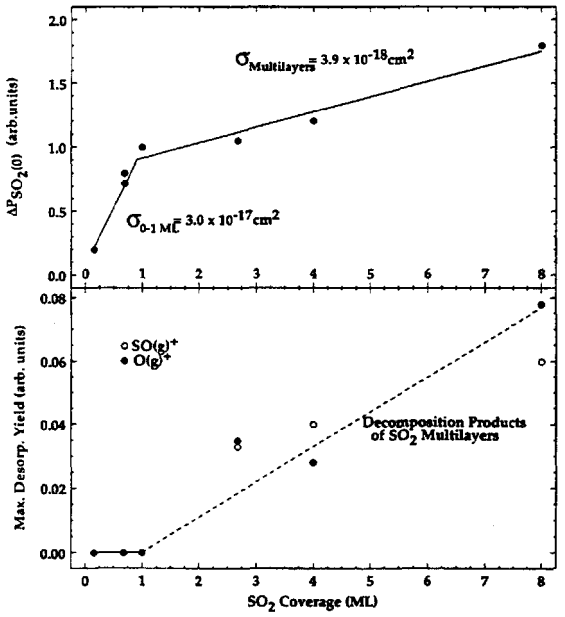

Figure 11. Upper panel: Initial desorption rate of SO_2 as a function of initial coverage. The solid lines represent fits to data according to eq 2. Lower panel: The maxima of the time-dependent SO^+ and O^+ signals as a function of initial SO_2 coverage. The electron energy was 54 ± 1 eV.

is stimulated desorption of SO_2 with a cross section of 3.6 ± 0.8 × 10^{-17} cm^2. Between 1 and 2 ML the cross section increases 3-fold, but then it becomes constant at 1.0 ± 1 × 10^{-16} cm^2 up to eight layers. The results described above clearly indicate that both desorption and dissociation make important contributions in the multilayer regime.

3.2.2. Products Ejected into the Gas Phase. In this section, we concentrate on the products that desorb during the irradiation of SO_2. As for Figure 3, Figure 10 shows, for 54 ± 1 eV electrons and three coverages, the time-dependent SO_2^+ signals. A semilogarithmic plot of the 8 ML data (not shown) is nonlinear and $\sigma_f = 4.0 \times 10^{-18}$ cm^2 fits the later times.

The *initial* SO_2 desorption rate, $\Delta P_{SO_2(0)}$, is related to the initial coverage, θ(0), according to:[30]

$$\Delta P_{SO_2(0)} = n\sigma(E)\theta(0) \qquad (6)$$

The top panel in Figure 11 shows the initial SO_2 pressure rise, $\Delta P_{SO_2(0)}$, as a function of initial SO_2 coverage, θ(0). $\Delta P_{SO_2(0)}$ has been normalized to the 1 ML case. Between 0 and 1 ML, $\Delta P_{SO_2(0)}$ increases linearly with coverages indicating that the cross section for stimulated desorption is constant. Assuming eq 6 is applicable to θ(0) ≤ 1, the initial cross section is 3.0 ± 0.8 × 10^{-17} cm^2.

For θ(0) ≥ 1 ML, the SO_2 desorption rate increases, but the cross section drops by an order of magnitude. Assuming eq 6 applies, $\sigma_i = 3.9 \pm 0.8 \times 10^{-18}$ cm^2 and refers, as does Figure 10, to neutral parent desorption, i.e., no account is taken of dissociation. This result for the initial cross section lies very close to that calculated from Figure 10 for longer irradiation times.

By contrast, the *total* cross section for loss of SO_2 as measured by postirradiation TPD areas (parent desorption and decomposition during electron irradiation) for multilayers is 2 orders of magnitude higher (1.0 ± 1 × 10^{-16} cm^2). Thus, when multilayers are irradiated with 54 ± 1 eV, electrons, *processes other than neutral desorption must dominate.*

In the previous sections, we have clearly established that dissociation occurs only when multilayers are adsorbed. Mass spectrometry and appearance potential measurements for *gas-phase* SO_2 show fragments at $m/e = 64, 48, 32$, and 16, attributed to SO_2^+, SO^+, S^+, and O^+, respectively.[31] After subtracting the contributions due to cracking of SO_2 and after normalizing to the initial SO_2^+ signal, the bottom panel in Figure 11 shows, for several initial SO_2 coverages, the maximum signals of SO^+ and O^+. Masses corresponding to desorption of SO_3, SO_4, and S_2O_6 species were searched for but not found.

There is no net SO^+ or O^+ signal below 1 ML. Above 1 ML, the O^+ signal appears promptly upon irradiation, but the SO^+ signal is delayed by 100 s, or more. This is probably related to the deviation from first-order desorption kinetics observed in the SO_2 desorption trace (Figure 10). Unfortunately, the net SO^+ and O^+ signals have a poor signal-to-noise ratio, which precludes quantitative kinetic analysis. Qualitatively, it is clear that electron-induced fragmentation occurs when physisorbed layers of SO_2 are present. It is very likely that ions are ejected from the surface during electron irradiation, particularly for coverages above 1 ML. We can say nothing about them with our present instrumentation.

4. Discussion

The main observations pertaining to the electron-induced chemistry of SO_2 layers on Ag(111) are as follows: (1) irradiation of the first (chemisorbed) layer results exclusively in stimulated desorption of SO_2 with an electron energy threshold of 18 eV; (2) SO_2 adsorbed on defect sites is not active for stimulated desorption; and (3) irradiation of physisorbed layers results in decomposition and desorption of SO_2 with a total cross section that is independent of coverage. Based on these observations, we discuss here the low-energy electron-induced processes occurring in the chemisorbed and physisorbed layers and compare them qualitatively with the effects induced by photons.

4.1. Chemistry Induced in Monolayers. It is well-known that charged particles (electrons and ions) can excite and induce the dissociation of molecular species adsorbed on transition metal and semiconductor surfaces.[8,10-13,32-34] The low-energy electron-induced effects that could lead to bond breakage in the Ag–SO_2 complex are (i) electron attachment, (ii) intramolecular electronic excitation, particularly to the lowest unoccupied molecular orbital, LUMO, of the adsorbate–substrate complex, via scattering of the incident electron, and (iii) positive ion formation by electron impact. We shall consider these three separately.

4.1.1. Electron Attachment. Electron attachment can be the result of interaction, with the adsorbed species, of incident electrons or secondary electrons that are generated in the substrate.[32] The electron affinity of SO_2 is high (1.12 eV) and SO_2^- is a very stable negative ion.[35] Electron beam mass spectrometry studies of low-energy dissociative electron attach-

ment (2.5–9.5 eV) of gas-phase SO_2 indicates the formation of O^-, SO^-, and S^- species.[36] The resonant attachment energies reported by Orient and Srivastava[36] are 4.3 eV (8×10^{-18} cm^2) and 7.1 eV (2×10^{-18} cm^2) for O^-; 4.0 eV (3×10^{-19} cm^2), 7.5 eV (3×10^{-20} cm^2), and 8.9 eV (3×10^{-20} cm^2) for S^-; and 4.7 eV (1×10^{-17} cm^2) and 7.5 eV (5×10^{-19} cm^2) for SO^-. For electron energies greater than 9 eV, the attachment cross sections were not very important. Since SO_2 is weakly held on Ag(111), we would expect attachment thresholds to be somewhat lower, because of anion stabilization, than those found in the gas phase. But, using electrons with incident energies lower than 18 eV, we found no induced chemistry, not even desorption, in the first layer ($\sigma \leq 10^{-20}$ cm^2) and, therefore, must consider other alternatives.

One alternative, hot electrons generated in the substrate, can also be ruled out here. As mentioned earlier, one interpretation of Figure 8 is that the 4.2-eV peak separation (152.0–147.8 eV) represents an electron energy loss process, e.g., the excitation of either Ag bulk plasmons (3.97 eV) or excitation of electrons from the 4d band (3.9 eV). These excitations could generate hot electrons leading to Ag–SO_2 bond cleavage via electron attachment. Such processes, in particular, bulk plasmon excitation, are important in the *photon-driven* desorption of SO_2 from Ag(111).[19a,b] The cross section for such processes is 3 orders of magnitude smaller than what we observe here ($2.8 \pm 0.2 \times 10^{-20}$ cm^2 for 3.8-eV photons[19]). We conclude that hot electron attachment makes a negligible contribution. Because photon-produced hot electrons do appear to control the desorption at lower energies, we are currently developing a variable energy photoelectron source to investigate the ESD of SO_2/Ag(111) with very low-energy electrons (0.5–20.0 eV), where attachment and plasmon excitation are expected to play important roles.

4.1.2. Intramolecular Excitation. Another path, electron excitation to unoccupied molecular orbitals in the adsorbate–substrate complex, should also be considered. Ultraviolet photoelectron spectroscopy (UPS) of SO_2/Ag(110)[23,27] shows that the gas-phase SO_2 LUMO, $3b_1$,[38] is filled, i.e., becomes the highest occupied molecular orbital, HOMO, and is located approximately 1.5 eV below the Fermi level. The work function for Ag(110) is 4.5 eV; therefore, the HOMO for the adsorbate–substrate complex lies approximately 6 eV below the vacuum level. We measured (not shown) the UP spectrum for SO_2 on Ag(111) and obtained results like those of Outka and Madix.[23] With respect to the *vacuum level*, the transition energies from the orbitals of the adsorbate–substrate complex are: $3b_1$ (6.7 eV); $8a_1$ (8.7 eV); $1a_2$ and $5b_2$ (10.7 eV); 2b1, $7a_1$, and $4b_2$ (12.5 and 14.5 eV); and $6a_1$ (18.9 eV).[37,38]

We also measured (not shown) the electron energy loss (EEL) spectrum for a 100-eV incident beam. For one monolayer, the only distinguishable loss peaks were at 19 ± 1 eV, near the threshold for the electron-stimulated processes, and at 3.8 eV (plasmon). We conclude from this data that energy losses, corresponding to energetically possible *intramolecular* excitations to unfilled molecular orbitals above the occupied $3b_1$ molecular orbital, do not make measurable contributions to the energy loss spectrum. By inference, we conclude that detectable electron-stimulated surface chemistry does not arise because of such intramolecular transitions.

The proximity of the 19-eV electron energy loss to the threshold for electron stimulated chemistry (Figure 4) is suggestive. For gaseous SO_2, there is a strong molecular shape resonance involving a transition from the $6a_1$ molecular orbital to Rydberg states centered at ~19 eV, as determined from photoabsorption measurements near the sulfur K and L edge[39] and extreme ultraviolet photon absorption measurements.[40] Although such transitions may be involved in the ESD of chemisorbed SO_2 from Ag(111), the next section describes another likely contribution.

4.1.3. Positive Ion Formation. From UPS results,[23,37,38] the binding energy of the $6a_1$ sulfur core molecular orbital is 18.7 eV, near the measured threshold for ESD. Thus, we propose that direct ionization of the $6a_1$ orbital is a major contributor to the excitations responsible for the SO_2 desorption.

TABLE I: Electron Stimulated Desorption Cross Sections

initial coverage	total cross section (cm^2)	neutral SO_2 desorption cross section (cm^2): pressure decay	neutral SO_2 desorption cross section (cm^2): initial rate (eq 2)
up to monolayer	3.6×10^{-17}	4.0×10^{-17}	3.0×10^{-17}
multilayers (2–8 ML)	1.1×10^{-16}	4.0×10^{-18}	3.9×10^{-18}

Transient ionic species, particularly those formed from weakly held species, are very susceptible to desorption and have been generically treated by Antoniewicz for electron- and photon-stimulated desorption.[41] In the case of SO_2 on Ag(111), the description is as follows: An SO_2–Ag complex interacts with an incident electron beam and undergoes a Franck–Condon transition[42] from the ground electronic state to a bound positive ion state of SO_2. The positive ion is attracted toward the surface via image charge forces and, after a short time interval (10–100 fs), an electron from bulk Ag tunnels to the SO_2, neutralizing it and returning it to the electronic ground state. The nascent neutral SO_2 finds itself significantly closer to the Ag than the equilibrium adsorbate–substrate distance and, therefore, on a repulsive potential energy surface. Depending on the Ag–S separation when quenching occurs, the SO_2 may be able to escape the ground-state attractive Ag–SO_2 potential and desorb as a *neutral* molecule.

The particular importance of the $6a_1$ orbital can be described, speculatively, as follows. The tunneling rate of an electron between the substrate and the adsorbate depends on the energetic position and spatial overlap of the molecular orbitals of the adsorbate with the band structure of the substrate. The band structure of clean Ag(111)[43] is characterized by Ag 5s and 4d bands localized between 4.7 and 12.3 eV, and 8.3 and 12.3 eV, respectively, below the vacuum level. The valence molecular orbitals of chemisorbed SO_2 align with the band structure of the substrate in order to reach equilibrium. Interestingly, the $6a_1$ molecular orbital (transition energy at 18.9 eV), localized on the sulfur (3s) is energetically well below the Ag(111) 5s and 4d bands. We propose that, because the nascent ionized $6a_1$ molecular orbital has small overlap with the substrate bands compared to ions formed using higher lying SO_2 orbitals, quenching is slower for ionized $6a_1$. This increased lifetime allows the SO_2^+ to move closer to the surface before quenching. Thus, the cross section for desorption is higher.

4.1.4. Absence of Dissociation. From Table I, for one monolayer, it is evident that the cross sections calculated using postirradiation TPD areas (total loss) and initial desorption rates (loss as SO_2) are consistent. This data strongly indicates that *neutral* SO_2 desorption dominates up to monolayer coverage.

The absence of dissociation in the chemisorbed monolayer is very interesting. In the gas phase, appearance potentials for the formation of SO_2 fragments are as follows: SO^+ and O (16.2 eV), S^+ and 2O (22.6 eV), S and O_2^+ (22.03 eV), S^+ and O_2 (17.48 eV), and S and O_2 (17.99 eV).[44] Our incident electron energy is capable of initiating all these ionizations, yet we do not observe fragmentation products, either retained on the surface or ejected into the gas phase. We suppose that the quenching time scale, while long enough to lead to desorption, is too short for dissociation to occur with measurable probability. Furthermore, we suppose that the ionic state is quenched by a Franck–Condon transition to a position on the ground-state potential energy surface that has insufficient vibrational excitation to dissociate.

For our system, these ionizations might lead to some parent desorption; we cannot rule it out, but their contribution is not required. While some of the appearance potentials are near the

extrapolated threshold for molecular desorption, their gas-phase cross section is 2×10^{-17} cm^2,[44] somewhat lower than we observe here, where we expect quenching to be competitive, i.e., it appears unlikely that these dominate on the surface.

4.2. Chemistry Induced in Multilayers. In passing from monolayers to multilayers, strong differences are observed. These are related to reduced quenching (longer ionic lifetimes), an effect that includes both charge and energy transfer and decreases sharply with increasing separation between the excited molecule and the substrate.[32,45] Consequently, more extensive nuclear motion will occur for excited molecules in physisorbed layers and can lead to fragmentation, as observed here. For example, the photolysis rate of chemisorbed methyl iodide on Pt(111)[46] and Ag(111)[47] is slower than for the corresponding physisorbed layers.

Above 1 ML (Figure 9), the total cross section for electron-induced chemistry is independent of coverage, indicating the substrate loses its influence—substrate quenching becomes negligible, adsorbate dissociation processes become competitive, and as discussed below, ionic desorption probably becomes important. There is ample evidence for electron-induced decomposition for multilayers: (1) At the QMS, O^+ and SO^+, not attributable to SO_2 cracking in the mass spectrometer, are detected during irradiation and their yields increase with SO_2 coverage. (2) Atomic sulfur is present after TPD to 500 K.

Assuming that electron-induced decomposition and desorption of the parent are independent processes, the total cross section, σ(total), can be expressed as a sum

$$\sigma(\text{total}) = \sigma_1 + \sigma_2 + \sigma_3 \qquad (7)$$

where σ_1 is the cross section for neutral parent desorption, σ_2 the cross section for dissociation, and σ_3 the cross section for all other processes that contribute to the loss of SO_2 (e.g., parent ion formation followed by desorption). Compared to monolayer coverages where $\sigma(\text{total}) = \sigma_1$, the description of multilayers requires a major contribution from $\sigma_2 + \sigma_3$. As indicated in Table I, postirradiation TPD areas provide a measure of σ(total), 1.1×10^{-16} cm^2, whereas the pressure rise of SO_2 provides a measure of σ_1 (4.0×10^{-18} cm^2). Thus, in this case, σ(total) is dominated by processes other than *neutral desorption*. In the following paragraphs we discuss the possible contributions of dissociation and parent ion desorption.

First, we consider possible mechanisms for intramolecular bond breaking. This can be initiated by either electron attachment to or electron ionization of physisorbed SO_2. As mentioned above, dissociative electron attachment (DEA) to gaseous SO_2 has a cross section of the order of 10^{-18} cm^2 using electrons with incident kinetic energy of 4.0–8.9 eV.[36] Furthermore, the DEA cross section *decreases* with electron energy above 9.0 eV. We find, using 54 ± 1 eV electrons, a cross section 100 times higher ($\sim 10^{-16}$ cm^2). Assuming that, within a multilayer, SO_2 has physical and electronic properties like those in the gas phase, we take such a high decomposition cross section as indicating that electron-induced decomposition of physisorbed SO_2 is not dominated by dissociative electron attachment but by ionization.

It is interesting that, in the gas phase,[44] 40-eV electrons lead to a total cross section (parent and fragment ion formation) of 1.9×10^{-16} cm^2, fortuitously close to the total cross section we find for multilayers. Partial cross sections for the formation of SO_2^+, SO^+, and S^+ or O_2^+ are 1.0×10^{-16}, 6×10^{-17}, and 1.9×10^{-17} cm^2, respectively.[43] We suggest that SO_2^+ formation dominates the multilayer chemistry (1×10^{-16} cm^2), and that both subsequent reactions with neighboring SO_2 and SO_2^+ desorption are responsible for the observation that $\sigma(\text{total}) \gg \sigma_1$ for multilayers. A revision of our apparatus is called for, one which would allow quantitative distinction between ion and neutral desorption.

To explain the apparent increase in the loss of chemisorbed SO_2 when multilayers are adsorbed (Figures 5 and 6), we offer the following thermodynamic argument based on Ag–SO_2 and Ag–S bond strengths. Atomic sulfur cannot be thermally desorbed from Ag at temperatures below 950 K, whereas molecular SO_2 desorbs at 180 K. Thus, we propose that an active ionic sulfur containing species, e.g., SO_2^+, SO^+, or S^+, is formed in multilayers and some fraction is scattered toward the surface. Dissociation, neutralization, and very strong Ag–S bonds form, and as a secondary result, SO_2 is displaced either into the gas phase or into a physisorbed state. Thus, in postsaturation TPD the intensity of the chemisorbed SO_2 is lower.

4.3. Comparison to Photochemistry. *4.3.1. Positive versus Negative Ion Formation.* It is of interest to compare photon[19a,b] and electron-induced desorption of chemisorbed SO_2 on Ag(111). For 54-eV electrons and coverages up to one monolayer, we observe a cross section of $3.6 \pm 0.8 \times 10^{-17}$ cm^2 and have described the process as dominated by ionization to *positive ion states* of the adsorbate followed by quenching to repulsive regions of the adsorbate–substrate potential energy curve. By comparison, we observed a much lower cross section for 3.8-eV photon-stimulated desorption (PSD), $\approx 10^{-20}$ cm^2. This process was interpreted in terms of attachment of photoexcited *substrate* electrons to chemisorbed SO_2.[19a,b] A quantitative comparison of these cross sections is not possible since our electron fluences are upper limits and since the photon-generated hot electron fluence is not known. Yet, many qualitative comparisons can be made.

It is interesting that both electrons and photons stimulate desorption of parent SO_2, yet the excitation mechanisms are different. According to our interpretation, electrons in the range 18–54 eV directly ionize the adsorbate $6a_1$ core level molecular orbital, and upon neutralization of the positive ion, the undissociated neutral parent desorbs. Under the influence of 3.8-eV photons, the mechanism is indirect; photons must be absorbed in the metal and subvacuum hot electrons must attach themselves to the adsorbate, forming an anion. The latter neutralizes by tunneling, and again, the undissociated neutral parent desorbs.

We now discuss the 3 orders of magnitude difference in the average cross sections for electrons (10^{-17} cm^2) and photons (10^{-20} cm^2). As noted above, one obvious distinction is that the photon-induced process must involve the cross sections for hot electron production and for transport to the surface, whereas these are not considerations in the electron-induced process. Beyond this, it is also of interest to consider how anions and cations might behave differently. A positive ion will have a smaller electron cloud than its neutral counterpart, whereas a negative ion will be larger. These sizes will influence the strength of the attractive image forces; they will be larger for the smaller, more localized, positive ion. Within the framework of the Antoniewicz model and assuming the quenching times are about the same, the positive ion will relax to the ground-state potential with a shorter S–Ag separation and, thus, will experience a greater repulsion after arriving on the ground-state potential. Up to some limit, dictated by the amount of energy needed to desorb the parent, this would result in higher cross sections for desorption induced by positive ion versus negative ion formation.

Quenching probabilities for positive and negative ions also probably differ since different adsorbate orbitals are involved, and there is no reason to expect their overlap with substrate orbitals to be the same. Positive ion formation involves removing an electron, leaving a hole, at the adsorbate. For a deep valence ionization as proposed here, overlap with the substrate band structure is probably lower than for holes in higher lying orbitals. For electron attachment, we expect occupation of states between the Fermi level and vacuum and relatively strong overlap with the substrate orbitals. Thus, we anticipate a higher quenching probability for the anion state than for the hole state.[41,43]

4.3.2. Initial and Final Cross Section For Stimulated Desorption. Up to monolayer coverage, there is strong evidence that the desorption cannot be described as a single first-order process (Figures 2b and 3b), but that two first-order processes (fast and

slow) are adequate. These results may be interpreted to indicate structurally different chemisorbed (weakly) SO_2 species with different electron-stimulated cross sections of 3.2×10^{-16} cm^2 and 4.0×10^{-17} cm^2, respectively. This subject has been treated in detail recently;[19b] in pulsed laser desorption of monolayer SO_2 from Ag at 100 K, at least two cross sections differing by an order of magnitude were required to fit the data. Directly relevant to the work described here, the initial cross section for photon-driven desorption from a monolayer of SO_2 on Ag(111) was 10-fold higher than that measured after 10% of the SO_2 was removed. Importantly, the cross section could be increased, simply by annealing the remaining SO_2, i.e., at constant coverage, the cross section is sensitive to the local details of the adsorbate–substrate structure. Some insight comes from organometallic complexes; three modes of SO_2 bonding to mononuclear transition metal complexes have been identified by infrared spectroscopy: η_1-planar, η_1-pyramidal and η_2 (in which bonding involves the p orbitals of sulfur and one oxygen atom). These various bonding configurations have characteristic S–O stretching frequencies.[20a] Sun et al.[19b] propose that SO_2 can adsorb in at least two different configurations, and more importantly, that photon activation drives both desorption and reorientation into less active configurations. While the states involved are different, adsorbate reorientation may be an important factor in our work as well. Further speculation is unwarranted until spectroscopic evidence is obtained, perhaps by HREELS or NEXAFS.

5. Conclusions

The results presented in this paper can be summarized as follows:

1. For monolayers, electron irradiation of SO_2 results in stimulated neutral parent desorption, but no dissociation. There is an electron energy threshold near 18.0 ± 0.8 eV corresponding to ionization of the $6a_1$ molecular orbital of adsorbed SO_2. At 54 eV, the cross section measured by post irradiation TPD areas is of order 10^{-17} cm^2.

2. For multilayers, intramolecular SO_2 dissociation and parent ion desorption become important. The total cross section for loss of SO_2 is $\approx 10^{-16}$ cm^2, while that for neutral parent desorption is 5×10^{-18} cm^2. These cross sections are independent of coverage within the multilayer regime.

3. Comparing the monolayer and multilayer regimes, differences in the electron-induced chemistry are attributed to a greater role for electronic quenching in the former.

4. A qualitative comparison of electron- and photon-stimulated desorption of SO_2 on Ag(111) indicates a number of similarities, even though the detailed excitation and quenching processes differ. While the cross sections are higher for electrons, there is evidence in both for at least two adsorbate structures with distinctly different responses.

Acknowledgment. Support by the National Science Foundation, Grant CHE9015600 and by the Robert A. Welch Foundation is gratefully acknowledged. The authors thank X.-Y. Zhu, Martin Wolf, X.-L. Zhou, and Z.-J. Sun for stimulating discussions. In addition, L.A.P. acknowledges support by the Promethium Chapter of Iota Sigma Pi—National Honor Society for Women in Chemistry.

References and Notes

(1) Zhou, X. L.; Zhu, X. Y.; White, J. M. *Surf. Sci. Rep.* **1991**, *13*, 77.
(2) Chuang, T. J. *Surf. Sci. Rep.* **1983**, *3*, 1.
(3) Ho, W. *Comments Condens. Matter Phys.* **1988**, *13*, 293.
(4) Basu, P.; Chen, J. G.; Ng, L.; Colaianni, M. L.; Yates, J. T., Jr. *J. Chem. Phys.* **1988**, *89*, 2406.
(5) *Desorption Induced by Electronic Transitions DIET I*; Tolk, N. H., Traum, M. M., Tully, J. C., Madey, T. E., Eds.; Springer: Berlin, 1983.
(6) *Desorption Induced by Electronic Transitions DIET II*; Brenig, W., Menzel, D., Eds.; Springer: Berlin, 1985.
(7) Zhou, X.-L.; White, J. M. *J. Chem. Phys.* **1990**, *92*, 5612.
(8) Castro, M. E.; Pressley, L. A.; White, J. M. *Surf. Sci.* **1991**, *256*, 227.
(9) Zhou, X.-L.; Coon, S. R.; White, J. M. *J. Chem. Phys.* **1990**, *92*, 1498.
(10) *Photon, Beam and Plasma Stimulated Chemical Processes at Surfaces*; Donnelly, V. M., Herman, I. P., Hirose, M., Eds.; MRS Symposium Proceedings; Materials Research Society: Boston, 1987.
(11) Zhou, X.-L.; Castro, M. E.; White, J. M. *Surf. Sci.* **1990**, *238*, 215.
(12) Zhou, X.-L.; Blass, P. M.; Koel, B. E.; White, J. M. *Surf. Sci.*, in press.
(13) Zhou, X.-L.; Blass, P. M.; Koel, B. E.; White, J. M. *Surf. Sci.*, in press.
(14) Zhou, X.-L.; White, J. M. *J. Phys. Chem.*, submitted for publication.
(15) Osgood, R. E. *Annu. Rev. Phys. Chem.* **1983**, *34*, 77.
(16) Hanley, L.; Guo, X.; Yates, J. T., Jr. *Surf. Sci.* **1990**, *232*, 129.
(17) Ehrlich, D. J.; Tsao, T. J. *J. Vac. Sci. Technol. B* **1983**, *1*, 969.
(18) Lloyd, K. G.; Roop, B.; Campion, A.; White, J. M. *Surf. Sci.* **1989**, *214*, 227.
(19) (a) Castro, M. E.; White, J. M. *J. Chem. Phys.* **1991**, *95*, 6057. (b) Sun, Z.-J.; Gravelle, S.; Mackay, R. S.; Zhu, X.-Y.; White, J. M. To be published.
(20) (a) Ryan, R. R.; Kubas, G. J.; Moody, D. C.; Eller, P. G. In *Structure and Bonding*; Clarke, M. J., Goodenough, J. B., Hemmerich, J. A., Ibers, J. A., Jorgensen, C. K.; Neilands, J. B., Reinen, D., Weiss, R., Williams, R. J. P., Eds.; Springer-Verlag: Berlin, 1981; Vol. 46. (b) Okabe, H. *Photochemistry of Small Molecules*; Wiley: New York, 1978; and references therein.
(21) Cox, R. A. *J. Phys. Chem.* **1972**, *76*, 814.
(22) Skotnick, P. A.; Hopkins, A. G.; Brown, W. W. *J. Phys. Chem.* **1975**, *79*, 2450.
(23) (a) Outka, D. A.; Madix, R. J. *Surf. Sci.* **1984**, *137*, 242. (b) Ahner, J.; Effendy, A.; Vajen, K.; Wassmuth, H.-W. *Vacuum* **1990**, *41*, 98.
(24) Outka, D. A.; Madix, R. J.; Di Maggio, G. L. *Langmuir* **1986**, *2*, 406.
(25) Koel, B. E.; Peebles, D. E.; White, J. M. *Surf. Sci.* **1983**, *125*, 709.
(26) Blass, P. M.; Zhou, S.-L.; White, J. M. *Surf. Sci.* **1989**, *215*, 74.
(27) Madey, T. E.; Yates, J. T., Jr. *J. Vac. Sci. Technol.* **1971**, *8*, 525.
(28) Salmeron, M.; Baro, A. M.; Rojo, J. M. *Phys. Rev.* **1976**, *B13*, 4348.
(29) Saas, J. K.; Laucht, H.; Kliewer, K. L. *Phys. Rev. Lett.* **1975**, *25*, 1461.
(30) Zhou, X.-L.; Coon, S.; White, J. M. *J. Chem. Phys.* **1990**, *92*, 1504.
(31) Reese, R. M.; Dibeler, V. H.; Franklin, J. L. *J. Chem. Phys.* **1958**, 880.
(32) Avouris, Ph.; Walkup, R. E. *Annu. Rev. Phys. Chem.* **1989**, *40*, 173.
(33) Hoflund, G. B. *Scanning Electron Microsc.* **1985**, *4*, 131.
(34) Ramsier, R. D.; Yates, J. T., Jr. *Surf. Sci. Rep.* **1991**, *12*, 246.
(35) Hasted, J. B.; Mathur, D. *Electron-Molecule Interactions and Their Applications*; Christophorou, L. G., Ed.; Academic Press: New York, 1984; Vol. I, p 451.
(36) Orient, O. J.; Srivastava, S. K. *J. Chem. Phys.* **1983**, *78*, 2949.
(37) Castro, M. E. Dissertation, University of Texas at Austin, 1991.
(38) Hillier, I. H.; Saunders, V. R. *Mol. Phys.* **1971**, *22*, 193.
(39) Bodeur, S.; Esteva, J. M. *Chem. Phys.* **1985**, *100*, 414.
(40) Robert, C. Y.; Judge, D. L. *J. Chem. Phys.* **1981**, *74*, 3804.
(41) Antoniewicz, P. R. *Phys. Rev.* **1980**, *B21*, 3811.
(42) Shimamura, I.; Takayanagi, K., Eds. *Electron-Molecule Collisions*; Plenum: New York, 1984.
(43) Papaconstantopoulos, D. A. *Handbook of the Band Structure of Elemental Solids*; Plenum Press: New York, p 167.
(44) Smith, O. I.; Stevenson, J. S. *J. Chem. Phys.* **1981**, *74*, 6777.
(45) Person, B. N. J.; Avouris, Ph. *J. Chem. Phys.* **1983**, *79*, 5156.
(46) Liu, Z.-M.; Akhter, S.; Roop, B.; White, J. M. *J. Am. Chem. Soc.* **1988**, *110*, 8708.
(47) Zhou, X.-L.; White, J. M. *Surf. Sci.* **1991**, *241*, 270.